Peter Benner   Judith Schneider

Uncertainty Quantification for Maxwell's Equations Using Stochastic Collocation and Model Order Reduction

Peter Benner   Judith Schneider

Uncertainty Quantification for Maxwell's Equations Using Stochastic Collocation and Model Order Reduction

MAX–PLANCK–INSTITUT
FÜR DYNAMIK KOMPLEXER
TECHNISCHER SYSTEME
MAGDEBURG

Abstract

Modeling and simulation are important for the design process of new semiconductor structures. Difficulties proceed from shrinking structures, increasing working frequencies, and uncertainties of materials and geometries. Therefore, we consider the time-harmonic Maxwell's equations for the simulation of a coplanar waveguide with uncertain material parameters. To analyze the uncertainty of the system, we use stochastic collocation with Stroud and sparse grid points. The results are compared to a Monte Carlo simulation. Both methods rely on repetitive runs of a deterministic solver. Hence, we compute a reduced model by means of proper orthogonal decomposition to reduce the computational cost. The Monte Carlo simulation and the stochastic collocation are both applied to the full and the reduced model. All results are compared concerning accuracy and computation time.

Contents

Author's addresses:

Peter Benner
Computational Methods in Systems and Control Theory, Max Planck Institute
for Dynamics of Complex Technical Systems, Sandtorstr. 1, 39106 Magdeburg Germany,
(benner@mpi-magdeburg.mpg.de)
Judith Schneider
Computational Methods in Systems and Control Theory, Max Planck Institute
for Dynamics of Complex Technical Systems, Sandtorstr. 1, 39106 Magdeburg Germany,
(judith.schneider@mpi-magdeburg.mpg.de)

1 Introduction

Nowadays, the design process of semiconductors is unimaginable without simulations of new micro and nano scale systems due to the expensive production of prototypes. However, the numerical simulation of systems which result from modeling of micro scale structures, see Figure 1 for an example of a wafer, is computationally demanding. Two aspects make the simulation even more complicated. One is the ongoing miniaturization of the structures, e. g., the technology improved from 90nm in 2004 to around 20nm in 2012, in combination with an increasing of the working frequencies. This implicates a high density of electric conductors and induces parasitic effects like crosstalk. In the past, the so called partial element equivalent circuit (PEEC) method [30] was used for numerical modeling of electromagnetic (EM) properties. Using the PEEC method, the problem is converted from the electromagnetic domain to
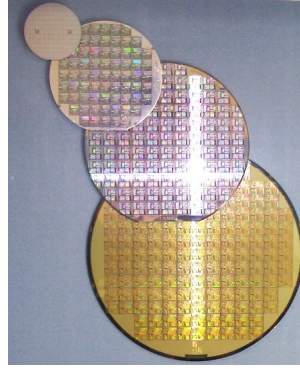
Figure 1: Wafer from 2 to 8 inches. (Source: `wikipedia.org`)

the circuit domain where traditional circuit solvers can be employed to analyze the equivalent circuit. However, at higher frequencies and for complicated geometries and more complex, e.g. inhomogeneous, materials, the PEEC method is not suitable. For such applications, differential field solvers like the Finite Element Method (FEM) are more feasible to compute the EM field by solving Maxwell's equations.
In the following, the electric field intensity $\boldsymbol{E}$ and the magnetic field intensity $\boldsymbol{H}$ are described by Maxwell's equations

$$\partial_t(\epsilon \boldsymbol{E}) = \nabla \times \boldsymbol{H} - \sigma \boldsymbol{E} - \boldsymbol{J}, \tag{1}$$

$$\partial_t(\mu \boldsymbol{H}) = -\nabla \times \boldsymbol{E}, \tag{2}$$

$$\nabla \cdot (\epsilon \boldsymbol{E}) = \rho, \tag{3}$$

$$\nabla \cdot (\mu \boldsymbol{H}) = 0, \tag{4}$$

where ρ is the charge density and $\boldsymbol{J}$ is the impressed current source. Furthermore, $\epsilon = \epsilon_r \cdot \epsilon_0$ (permittivity), $\mu = \mu_r \cdot \mu_0$ (permeability), and σ (electrical conductivity) are material dependent parameters. The equations are considered in a domain $G \subset \mathbb{R}^3$.
We decouple the full Maxwell's equations by exploiting the fact that $\nabla \times (\nabla \varphi) = 0$ for scalar

potentials φ and $\nabla \cdot (\nabla \times \boldsymbol{A}^*) = 0$ for vector potentials $\boldsymbol{A}^*$. Then (4) yields

$$\exists \boldsymbol{A}^* : \nabla \times \boldsymbol{A}^* = \mu \boldsymbol{H}.$$

Substituting into (2) leads to

$$\nabla \times (\boldsymbol{E} + \partial_t(\boldsymbol{A}^*)) = 0,$$

which implies the existence of a scalar potential φ such that

$$\boldsymbol{E} = -\nabla \varphi - \partial_t(\boldsymbol{A}^*).$$

By choosing $\boldsymbol{A} = \boldsymbol{A}^* + \int_{t_0}^t \nabla \varphi \, dt$ [37], we obtain $\boldsymbol{E} = -\partial_t(\boldsymbol{A})$, $\nabla \times \boldsymbol{A} = \nabla \times \boldsymbol{A}^*$, and the vector potential formulation of Maxwell's equations (1)-(4)

$$\nabla \times (\mu^{-1} \nabla \times \boldsymbol{A}) + \sigma \, \partial_t(\boldsymbol{A}) + \epsilon \, \partial_t^2(\boldsymbol{A}) = \boldsymbol{J}.$$

For a further simplification, we work with the time-harmonic form, i. e., we assume $\boldsymbol{A}$ to be given in the form $\boldsymbol{A} = \hat{\boldsymbol{A}} \cdot e^{i\omega t}$, where ω is the working frequency. With this assumption, the time derivatives simplify to

$$\partial_t(\boldsymbol{A}) = i\omega \cdot \boldsymbol{A}, \qquad\qquad \partial_t^2(\boldsymbol{A}) = -\omega^2 \cdot \boldsymbol{A}.$$

Therefore, the vector potential formulation can be written as

$$\nabla \times (\mu^{-1} \nabla \times \boldsymbol{A}) + i \, \omega \, \sigma \boldsymbol{A} - \omega^2 \, \epsilon \boldsymbol{A} = \boldsymbol{J}.$$

By replacing $\boldsymbol{E} = -\partial_t(\boldsymbol{A}) = -i\omega \boldsymbol{A}$ [3, 21], we obtain the time-harmonic Maxwell's equation

$$\nabla \times (\mu^{-1} \nabla \times \boldsymbol{E}) + i \, \omega \, \sigma \boldsymbol{E} - \omega^2 \, \epsilon \boldsymbol{E} = -i \, \omega \, \boldsymbol{J}, \tag{5}$$

for which the solution $\boldsymbol{E}$ lives in the space $X = \{\boldsymbol{E} \in H_{curl}^0(G) | \nabla \cdot (\epsilon \boldsymbol{E}) = \rho\}$, where

$$H_{curl}^0(G) := \{\boldsymbol{E} \in (L_2(G))^3 | \nabla \times \boldsymbol{E} \in (L_2(G))^3, \boldsymbol{E} \times \boldsymbol{n} = 0 \text{ on } \partial G\}$$

and

$$L_2(G) = \{u | \int_G u^2 d\boldsymbol{x} < \infty\}.$$

For the simulation, (5) is discretized by means of the finite element method. This will be further explained in section 5.

To allow for fluctuations in the processed materials, the material parameters are treated as uncertain parameters of the system. In this paper these uncertain parameters are ϵ_r, μ_r, and σ. Inaccuracies during the lithography which lead to variations of the feature structure sizes lead to another aspect that can no longer be neglected during the simulation. These geometric parameters will not be considered in this work. This aspect will be treated in the future.

For a variational analysis of the effect of uncertainties on the electromagnetic field, methods for uncertainty quantification (UQ) [20, 31] are required. The existing methods in this field can be divided into intrusive and non-intrusive methods. The motivation for non-intrusive methods is that in the cooperation with industrial partners the discretization of the system

equations is often done by a commercial tool and therefore has to be considered as a black box. In this case, intrusive UQ methods like stochastic finite elements [29], which would lead to a new discretization respecting the uncertainty in the system, can not be used. Therefore, we will employ non-intrusive approaches in order to design an algorithm that allows the use of EM field solvers for deterministic problems without accessing the source code. Possible non-intrusive methods are the well-known Monte Carlo (MC) simulation [22, 12], which yields arbitrary exactness but has a slow convergence, or the stochastic collocation approach [1, 2, 16, 36]. In our case, the results computed by MC serve as reference solutions. Considering stochastic collocation, the choice of collocation points is very important for the accuracy of the results on the one hand and the effectiveness of the method on the other hand. This will be further investigated in this work.

Another way of saving computation time is to replace the high dimensional discretized solution of (5) by a system of reduced order. Such systems can be computed by model order reduction (MOR). We use a reduced-order model (ROM) instead of the full-order model (FOM) for the MC and the collocation approach. This ROM is obtained by MOR via proper orthogonal decomposition (POD) [19, 32, 35, 15].

One of the first publications considering UQ for microelectronics is [17], where a projection based MOR method for variational analysis of RLC interconnect circuits was presented. In the last years, many people worked in this area. Stroud-based collocation has already been used for the statistical characterization of coupled voltages in [2]. In [16], sparse collocation methods with diverse kinds of sample points are applied to electromagnetic scattering by a two-dimensional cylinder with a uncertain number of wholes with uncertain size and location. The two choices of sample points, Stroud and sparse grids, are compared in [36] considering as example an elliptic equation.

Here, we combine components of the latter papers. We use Stroud points [34] and sparse grids [5] and apply the stochastic collocation to the time-harmonic Maxwell's equations in high-frequency range with uncertain material parameters. The use of non-intrusive methods is driven by the application described in section 2.

The combination of MOR and UQ is rarely studied up to now. One example is [28], where a projection based reduction of the state space and a reduction of the random space are applied to an electric network with uncertain capacitances, inductances, and conductances. Another one is [7], where a combination of reduced basis and stochastic collocation is applied to stochastic versions of the diffusion equation and the incompressible Navier-Stokes equations. In this work, we place value on reducing a parameter-affine system once, followed by a repetitive usage of the obtained ROM in the UQ method.

The paper is structured as follows. We describe our application, a coplanar waveguide with dielectric overlay, in section 2. The UQ methods of interest, Monte Carlo and stochastic collocation, as well as our different choices of collocation points are explained in section 3. We will give a short introduction to MOR by POD in section 4 and show the numerical results in section 5. A short conclusion is given in section 6.

3
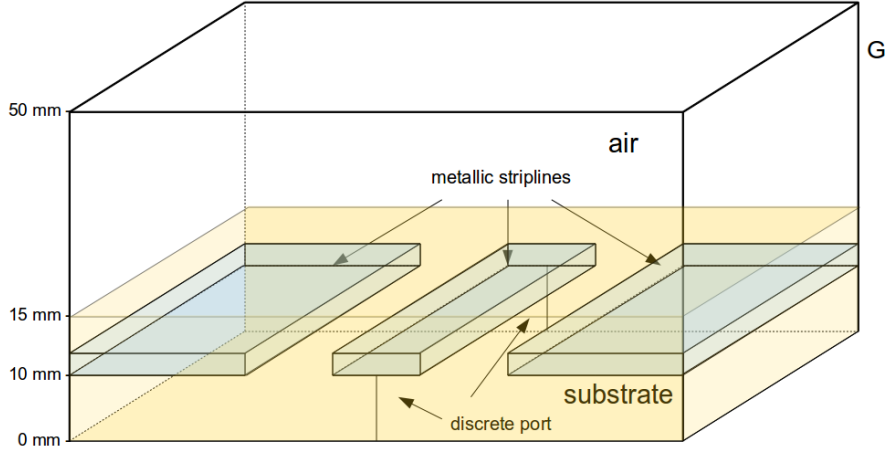
Figure 2: Coplanar waveguide.

2 Application: A Coplanar Waveguide

The application of interest is a coplanar waveguide with dielectric overlay which is shown in Figure 2. A detailed description of the coplanar waveguide (only with geometric parameters) can be found in the MOR wiki [23].

The model consists of three perfectly conducting striplines situated at a height of 10mm in a shielded box with perfect electric conductor (PEC) boundary. The system is excited at discrete port 1 and the voltage along port 2 is taken as output.

Below a height of 15mm there is a substrate, the rest of the box is filled with air. The uncertainties of the model are the material parameters ϵ_r, μ_r, and σ. As the relative permittivity ϵ_r and the conductivity σ have different means for substrate and air, we have to work with two sub-domains G_s (substrate) and G_a (air). That means, we split ϵ_r and σ and treat the system as a system with 5 uncertain parameters.

Due to physical reasons, the parameters have to be positive. Therefore, they are assumed to be log-normally distributed. The given means $\mathbb{E}(\boldsymbol{p}_j)$, standard deviations $std(\boldsymbol{p}_j)$, and the arguments $\boldsymbol{\mu}_j$ and $\boldsymbol{\sigma}_j$ for the log-normal distributions $\mathcal{LN}(\boldsymbol{\mu}_j, \boldsymbol{\sigma}_j^2)$ of the five parameters are given in Table 1. The assumed probability density function for parameter $\boldsymbol{p}_j$ is

$$f_j(x) := \frac{1}{\sqrt{2\pi}\boldsymbol{\sigma}_j x} \exp\left(-\frac{(\ln(x) - \boldsymbol{\mu}_j)^2}{2\boldsymbol{\sigma}_j^2}\right) \quad \text{for } x \in \mathbb{R}, \ x > 0.$$

We use the arguments $\boldsymbol{\mu}_j$ and $\boldsymbol{\sigma}_j$ to compute the Stroud and sparse grid points. Then we take the exponential of them as sample points, since the exponential of a normally distributed random variable is log-normally distributed.

4

j	$\boldsymbol{p}_j$	$\mathbb{E}(\boldsymbol{p}_j)$	$std(\boldsymbol{p}_j)$	$\boldsymbol{\mu}_j$	$\boldsymbol{\sigma}_j$
1	ϵ_r^s	4.40	10^{-2}	1.4816	0.0023
2	ϵ_r^a	1.07	10^{-2}	0.0676	0.0093
3	μ_r	1.00	10^{-2}	0.0000	0.0100
4	σ^s	0.02	10^{-4}	-3.9120	0.0050
5	σ^a	0.01	10^{-4}	-4.6052	0.0100

Table 1: Parameter information for the coplanar waveguide.

The time-harmonic Maxwell's equations (5) depending on five parameters can be written as

$$\nabla \times ((\mu_r\mu_0)^{-1}\nabla \times \boldsymbol{E}) + i\omega(\sigma^s\mathbb{1}_{G_s} + \sigma^a\mathbb{1}_{G_a})\boldsymbol{E} - \omega^2\epsilon_0(\epsilon_r^s\mathbb{1}_{G_s} + \epsilon_r^a\mathbb{1}_{G_a})\boldsymbol{E} = -i\omega\boldsymbol{J}, \quad (6)$$

where $\mathbb{1}_{G_s}$, $\mathbb{1}_{G_a}$ denote the indicator functions of sub-domain G_s, G_a, respectively.
In the next section, we explain the stochastic background and describe different choices of collocation points and their usage for the coplanar waveguide.

3 Non-Intrusive Uncertainty Quantification

Let $(\Omega, \mathcal{F}, \mathcal{P})$ be a probability space, where Ω is the set of all elementary events, $\mathcal{F}$ is a σ-algebra of subsets of Ω, and $\mathcal{P}$ is a probability measure on $\mathcal{F}$. Given a square integrable random variable $Y : \Omega \to \Gamma$, where $\Gamma = \mathbb{R}$ or $\mathbb{C}$, with probability density function f and an arbitrary function $g : \Gamma \to \mathbb{C}^d$ for a natural number d, we are interested in the computation of statistical quantities like the mean

$$\mathbb{E}\left(g(Y)\right) := \int_\Omega g(Y(\omega))d\mathcal{P}(\omega) \tag{7}$$

and the standard deviation

$$std\left(g(Y)\right) := \sqrt{\mathbb{E}\left(g(Y)^2\right) - (\mathbb{E}\left(g(Y)\right))^2} \tag{8}$$

of $g(Y)$. For practical computation, a numerical approximation of (7) and (8) is sometimes needed.
Non-intrusive methods are sampling techniques which rely on repetitive runs of a discrete solver. The most popular uncertainty quantification method is the MC simulation [22, 12]. The idea behind MC is the law of large numbers which describes the result of running the same experiment a large number of times. Given a realization $(\xi_1, \ldots, \xi_n)$ of a sample $(Y_1, \ldots, Y_n)$ of the random variable Y, the sample mean of $g(Y)$ is given by

$$m_n := \frac{1}{n}\sum_{i=1}^n g(\xi_i).$$

By the law of large numbers, we have $m_n \to \mathbb{E}\left(g(Y)\right)$ for $n \to \infty$. Hence, $m_n \approx \mathbb{E}\left(g(Y)\right)$ for large n.

5

Therefore, MC uses a randomly chosen realization $(\xi_1, \ldots, \xi_n)$ and equal weights for the approximation of $\mathbb{E}\left(g(Y)\right)$

$$\mathbb{E}\left(g(Y)\right) \approx \frac{1}{n} \sum_{i=1}^{n} g(\xi_i) \qquad \text{for large } n.$$

The convergence is proportional to $1/\sqrt{n}$, where n is the number of sampling points. Considering the coplanar waveguide in section 2, the vector of uncertain parameters $\boldsymbol{p}$ is a 5-dimensional vector of log-normally distributed random variables and $\boldsymbol{E}(\boldsymbol{p})$ is the function g we are interested in.

3.1 Stochastic Collocation

Another approach based on sampling is the stochastic collocation method. Its effectiveness depends strongly on the choice of collocation points. The idea is to approximate statistical quantities like the mean (7), by an (efficient) quadrature rule

$$\mathbb{E}\left(g(Y)\right) = \int_{\Gamma} g(x) f(x) dx \approx \sum_{i=1}^{n} g(\xi_i) w_i =: \hat{\mathbb{E}}\left(g(Y)\right).$$

Here, the realization $(\xi_1, \ldots, \xi_n)$, later called the sample points $\{\xi_i\}_{i=1}^{n}$, and the weights $\{w_i\}_{i=1}^{n}$ are determined by use of the probability density function f. Higher moments like the standard deviation can be approximated by use of $\hat{\mathbb{E}}\left(g(Y)\right)$

$$std\left(g(Y)\right) \approx \sqrt{\sum_{i=1}^{n}(g(\xi_i))^2 w_i - \left(\hat{\mathbb{E}}\left(g(Y)\right)\right)^2}.$$

Like MC, stochastic collocation requires only repetitive runs of an existing deterministic solver. The difference is the choice of sample points and weights. It is always possible to use a tensor product of a one-dimensional interpolation formula. For many parameters, this becomes very expensive. Therefore, we use two other options that suffer less from the curse of dimensionality. One way is to use only a part of the tensor grid, which is done by the Smolayk algorithm. The result is called a sparse grid. Another way to compute the points are the Stroud integration rules which yield a very small number of points and have a fixed accuracy. Both options are described below.

Stroud-3 Integration Rules

The Stroud-3 integration rule was introduced in 1957 by A. H. Stroud [34] and yields either beta or normally distributed points which are weighted by $1/n$, where n is the number of points. In our case only the normally distributed points are considered. This choice is motivated by the physics of the considered application, i. e., the fact that the parameters are assumed to be log-normally distributed, as explained in section 2.

(a) Stroud   (b) HGK sparse grid level 2   (c) HGK tensor grid
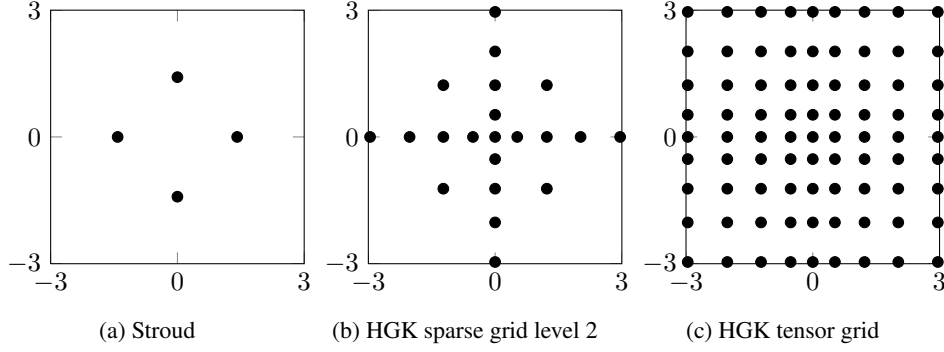
Figure 3: Comparison of Stroud, HGK sparse grid level 2 and tensor grid in 2 dimensions.

For a system with N parameters only $2N$ sample points are needed. The $j-$th component of the normally distributed points with mean $\boldsymbol{\mu}_j$ and standard deviation $\boldsymbol{\sigma}_j$ is in [2] given as

$$x_j^i = \boldsymbol{\sigma}_j \cdot z_j^i + \boldsymbol{\mu}_j,$$

where for $i = 2r - 1$, $i = 2r$, respectively and $r = 1, 2, \ldots, \lfloor N/2 \rfloor$

$$z_j^{2r-1} = \sqrt{2} \cos\left(\frac{(2r-1)j\pi}{N}\right), \qquad z_j^{2r} = \sqrt{2} \sin\left(\frac{(2r-1)j\pi}{N}\right).$$

If N is odd, then $z_j^N = (-1)^j$. Here, $\lfloor N/2 \rfloor$ is the biggest natural number smaller or equal than $N/2$.

Stroud-based stochastic collocation has been discussed in [2, 36]. The used Stroud-3 rule is exact for polynomials up to degree 3. It is optimal for systems with few parameters because of the very small number of sample points. Unfortunately, the accuracy is fixed, which makes this method inappropriate for higher order systems. Figure 3a shows the standard normally distributed Stroud points for a system with two parameters.

In case of the coplanar waveguide, Stroud yields $n = 10$ sample points $\{\boldsymbol{\xi}_i\}_{i=1}^{10}$ in the 5-dimensional parameter space.

Hermite Genz-Keister Sparse Grids

Sparse grids are constructed by the Smolyak algorithm [27, 33] which is a linear combination of product formulas. Every one-dimensional quadrature rule can be chosen and the linear combination preserves the interpolation properties of the univariate case for higher dimensions. We use a one-dimensional Hermite Genz-Keister (HGK) rule [9, 13] as starting point for the Smolyak algorithm. Genz and Keister [9] developed multidimensional Gauss-Hermite (GH) [14] schemes which have several nice features. As Gauss-Patterson rules (GP) [10, 16, 26] they are nested but in contrast to them they are computed on infinite regions. Furthermore, for a fixed order the number of grid points growths only exponentially. The advantage compared with a usual GH rule is the nestedness.

Due to the fact that they are computed after a difficult scheme, HGK rules do not exist for arbitrary numbers of generating points. The beginning is a one-point Gauss-Hermite rule which has degree 1. By adding new generators to that rule, we can achieve rules with degree 3, 15, 19, 29, 51, 63 and 67 [9]. The higher the level of the sparse grid, the higher the number of generating points of the underlying one-dimensional quadrature rule.

To illustrate the sparsity of sparse grids, Figure 3b shows the HGK sparse grid of level 2 (HGK 2) with $n = 21$ grid points and Figure 3c shows the corresponding tensor grid with $n = 81$ grid points for a standard normally distributed variable in two dimensions. In case of the coplanar waveguide, we use HGK sparse grids of levels 0, 1, and 2 which have 1, 11, and 81 points in the 5-dimensional parameter space.

In the next section we explain a POD-based MOR method.

4 Model Order Reduction

UQ via MC or stochastic collocation requires numerous full-order EM field solves which can be a time-consuming task for complicated 3D geometries. It is thus our goal to combine this approach with MOR for the time-harmonic Maxwell's equations (6) to reduce the computational cost. We need a ROM that preserves the statistical properties of the FOM.

In this work, we use a POD-based MOR like described in [15]. POD was first mentioned under this name in [19]. Its central issue is the reduction of data revealing the essential information with the aid of a few basis vectors. We will explain the close connection to the singular value decomposition (SVD) [11] of rectangular matrices in this section.

For a given matrix $Y = [y_1, \ldots, y_{m_2}] \in \mathbb{R}^{m_1 \times m_2}$ with rank $d \leq \min\{m_1, m_2\}$, the SVD ensures the existence of real numbers $\sigma_1 \geq \sigma_2 \geq \ldots \geq \sigma_d > 0$ and orthogonal matrices $U = [u_1, \ldots, u_{m_1}] \in \mathbb{R}^{m_1 \times m_1}$ and $V = [v_1, \ldots, v_{m_2}] \in \mathbb{R}^{m_2 \times m_2}$ such that

$$U^T Y V = \begin{pmatrix} D & 0 \\ 0 & 0 \end{pmatrix} =: \Sigma \in \mathbb{R}^{m_1 \times m_2}$$

with $D = \operatorname{diag}(\sigma_1, \ldots, \sigma_d) \in \mathbb{R}^{d \times d}$ and zero matrices of appropriate dimensions. For any $l \in \{1, \ldots, d\}$ the solution to

$$\max_{\tilde{u}_1, \ldots, \tilde{u}_l \in \mathbb{R}^{m_1}} \sum_{i=1}^{l} \sum_{j=1}^{m_2} |\langle y_j, \tilde{u}_i \rangle_{\mathbb{R}^{m_1}}|^2 \quad s.t. \quad \langle \tilde{u}_i, \tilde{u}_j \rangle_{\mathbb{R}^{m_1}} = \delta_{ij} \, for \, 1 \leq i, j \leq l$$

is given by the first l columns of U, $\{u_i\}_{i=1}^{l}$, which yields the POD basis of rank l. For a given $l \leq d$ the POD yields the best approximation of the columns of Y among all rank l approximations.

The vectors $y_1, \ldots, y_{m_2}$ are called snapshots, a designation which was first used in [32].

In our example, we need snapshots of the parameters which are then used to compute snapshots of the electrical field. We have several possibilities for the choice of snapshots. One could use either the Stroud or the HGK sparse grid sample points for the computation of the snapshots of the electrical field. Both choices do not yield useful reduced models.

In our example, we use 3 snapshots for every single parameter $\boldsymbol{p}_j$, namely $\boldsymbol{\mu}_j - 3\boldsymbol{\sigma}_j$, $\boldsymbol{\mu}_j$, and

$\boldsymbol{\mu}_j + 3\boldsymbol{\sigma}_j$. This choice is motivated by the fact that 99% of all realizations of a $\mathcal{N}(\mu, \sigma)$-distributed random variable lie in the interval $[\mu - 3\sigma, \mu + 3\sigma]$. Each of the 3^5 parameter snapshots yields a snapshot of the electrical field. These $\boldsymbol{E}$-snapshots are used for the POD.

5 Numerical Results

We show some numerical results for the coplanar waveguide in Figure 2, which are achieved by the previously explained collocation method. The discretization of the affine system (6) and the assembling of the matrices [8] is done in FEniCS [18] by use of Nédélec finite elements [24, 25]. In the finite element context, a weak solution of (6) is searched instead of a classical one. Therefore, we employ a variational formulation, i.e., we multiply (6) by a test function $\boldsymbol{v} \in H_{curl}(G) := \{\boldsymbol{v} \in (L_2(G))^3 \,|\, curl(\boldsymbol{v}) \in (L_2(G))^3\}$ and integrate over G. This leads to

$$\int_G \nabla \times ((\mu_r \mu_0)^{-1} \nabla \times \boldsymbol{E}) \boldsymbol{v} d\boldsymbol{x} + \int_G i\omega(\sigma^s \mathbb{1}_{G_s} + \sigma^a \mathbb{1}_{G_a}) \boldsymbol{E} \boldsymbol{v} d\boldsymbol{x}$$
$$- \int_G \omega^2 \epsilon_0 (\epsilon_r^s \mathbb{1}_{G_s} + \epsilon_r^a \mathbb{1}_{G_a}) \boldsymbol{E} \boldsymbol{v} d\boldsymbol{x} = - \int_G i\omega \boldsymbol{J} \boldsymbol{v} d\boldsymbol{x}.$$

Now the first integral is integrated by parts [4], which leads to

$$\int_G ((\mu_r \mu_0)^{-1} \nabla \times \boldsymbol{E})(\nabla \times \boldsymbol{v}) d\boldsymbol{x} - \int_{\partial G} (\mu_r \mu_0)^{-1}((\nabla \times \boldsymbol{E}) \times \boldsymbol{n}) \boldsymbol{v} ds$$
$$+ \int_G i\omega(\sigma^s \mathbb{1}_{G_s} + \sigma^a \mathbb{1}_{G_a}) \boldsymbol{E} \boldsymbol{v} d\boldsymbol{x} - \int_G \omega^2 \epsilon_0 (\epsilon_r^s \mathbb{1}_{G_s} + \epsilon_r^a s \mathbb{1}_{G_a}) \boldsymbol{E} \boldsymbol{v} d\boldsymbol{x} = - \int_G i\omega \boldsymbol{J} \boldsymbol{v} d\boldsymbol{x}.$$

For the boundary integral, it can easily be seen that

$$\int_{\partial G} (\mu_r \mu_0)^{-1}((\nabla \times \boldsymbol{E}) \times \boldsymbol{n}) \boldsymbol{v} ds = \int_{\partial G} (\mu_r \mu_0)^{-1}(\nabla \times \boldsymbol{E})(\boldsymbol{n} \times \boldsymbol{v}) ds,$$

which is equal to zero if $\boldsymbol{n} \times \boldsymbol{v} = 0$. Therefore, we obtain the weak formulation

$$\int_G ((\mu_r \mu_0)^{-1} \nabla \times \boldsymbol{E})(\nabla \times \boldsymbol{v}) d\boldsymbol{x} + \int_G i\omega(\sigma^s \mathbb{1}_{G_s} + \sigma^a \mathbb{1}_{G_a}) \boldsymbol{E} \boldsymbol{v} d\boldsymbol{x}$$
$$- \int_G \omega^2 \epsilon_0 (\epsilon_r^s \mathbb{1}_{G_s} + \epsilon_r^a \mathbb{1}_{G_a}) \boldsymbol{E} \boldsymbol{v} d\boldsymbol{x} = - \int_G i\omega \boldsymbol{J} \boldsymbol{v} d\boldsymbol{x}, \tag{9}$$

for all $\boldsymbol{v} \in H^0_{curl}(G)$.

The system is discretized by replacing the domain G by a finite dimensional closed subspace, in our case a finite element grid G_h with 18755 degrees of freedom (dofs). For $\boldsymbol{v}_1, \boldsymbol{v}_2 \in H^0_{curl}(G_h)$, $\mathbb{1}_{in}$ and $\mathbb{1}_{out}$ the indicator function for the input and output region, respectively,

9

and $l = a, s$, we define

$$A_{\mu_0} = \int_{G_h} (\mu_0^{-1} \nabla \times \boldsymbol{w})(\nabla \times \boldsymbol{v}) d\boldsymbol{x},$$

$$A_{\epsilon_0}^l = \int_{G_h} \epsilon_0 \mathbb{1}_{G_l} \boldsymbol{w} \boldsymbol{v} d\boldsymbol{x},$$

$$A^l = \int_{G_h} \mathbb{1}_{G_l} \boldsymbol{w} \boldsymbol{v} d\boldsymbol{x},$$

$$B = -\int_{G_h} i\omega \mathbb{1}_{in} \boldsymbol{v} d\boldsymbol{x},$$

$$C = \int_{G_h} \mathbb{1}_{out} \boldsymbol{v} d\boldsymbol{x}.$$

Hence, the affine discretized form of (9) is

$$\mu_r A_{\mu_0} \boldsymbol{e} - \omega^2 (\epsilon_r^s A_{\epsilon_0}^s + \epsilon_r^a A_{\epsilon_0}^a) \boldsymbol{e} + i\omega(\sigma^s A^s + \sigma^a A^a) \boldsymbol{e} = Bu, \qquad (10)$$
$$y = C\boldsymbol{e},$$

where the second equation describes the output behavior of the system, u is the input current and y the output voltage (both one-dimensional). Furthermore, the matrices $A_{\epsilon_0}^a$, $A_{\epsilon_0}^s$, A^a, and A^s have non-zero entries only on the corresponding sub-domain. We consider as working frequency $\omega = 0.6 \cdot 10^9$.

We want to approximate the mean and the standard deviation of the solution $\boldsymbol{e}(\boldsymbol{p}) \in H_{curl}^0(G_h)$ and the output $y(\boldsymbol{p})$ of (10) via

$$\mathbb{E}(\boldsymbol{e}(\boldsymbol{p})) \approx \sum_{i=1}^{n} \boldsymbol{e}(\boldsymbol{\xi}_i) w_i, \qquad std(\boldsymbol{e}(\boldsymbol{p})) \approx \sqrt{\sum_{i=1}^{n} |\boldsymbol{e}(\boldsymbol{\xi}_i)|^2 w_i - |\mathbb{E}(\boldsymbol{e}(\boldsymbol{p}))|^2},$$

$$\mathbb{E}(y(\boldsymbol{p})) \approx \sum_{i=1}^{n} y(\boldsymbol{\xi}_i) w_i, \qquad std(y(\boldsymbol{p})) \approx \sqrt{\sum_{i=1}^{n} |y(\boldsymbol{\xi}_i)|^2 w_i - |\mathbb{E}(y(\boldsymbol{p}))|^2},$$

using stochastic collocation with sample points $\{\boldsymbol{\xi}_i\}_{i=1}^n$ obtained by Stroud or HGK sparse grids with the corresponding weights w_i. For reasons of simplification, we will omit the $\boldsymbol{p}$-dependence of $\boldsymbol{e}$ and y in the following.

For the approximations computed via MC, $\mathbb{E}_{MC}(\boldsymbol{e})$, $std_{MC}(\boldsymbol{e})$, $\mathbb{E}_{MC}(y)$, and $std_{MC}(y)$, we compare the following errors for different choices of collocation points

$$err_{\mathbb{E}(\boldsymbol{e})}^{rel} := \left| \frac{\mathbb{E}(\boldsymbol{e}(\boldsymbol{x})) - \mathbb{E}_{MC}(\boldsymbol{e}(\boldsymbol{x}))}{\mathbb{E}_{MC}(\boldsymbol{e}(\boldsymbol{x}))} \right|,$$

$$err_{std(\boldsymbol{e})}^{rel} := \left| \frac{std(\boldsymbol{e}(\boldsymbol{x})) - std_{MC}(\boldsymbol{e}(\boldsymbol{x}))}{std_{MC}(\boldsymbol{e}(\boldsymbol{x}))} \right|,$$

$$err_{\mathbb{E}(y)}^{rel} := \left| \frac{\mathbb{E}(y) - \mathbb{E}_{MC}(y)}{\mathbb{E}_{MC}(y)} \right|,$$

$$err_{std(y)}^{rel} := \left| \frac{std(y) - std_{MC}(y)}{std_{MC}(y)} \right|.$$

10
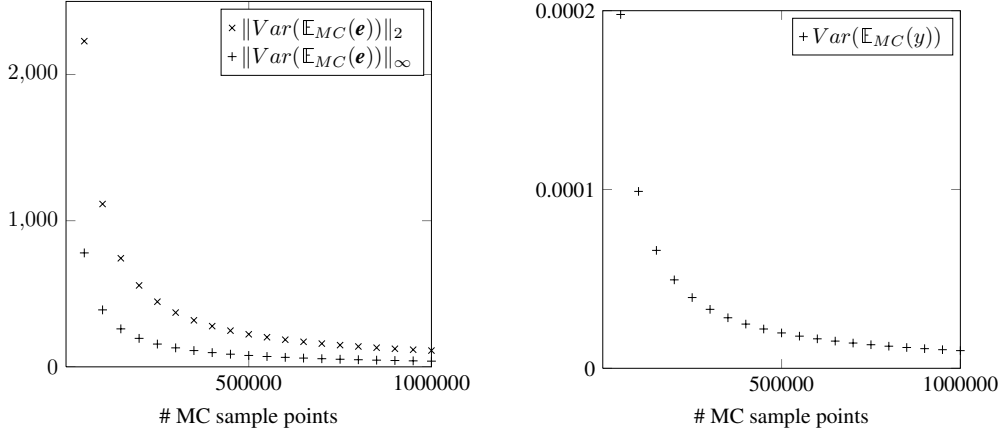
Figure 4: Monte Carlo convergence.

Method	$\|err^{rel}_{\mathbb{E}(e)}\|_2$	$\|err^{rel}_{\mathbb{E}(e)}\|_\infty$	$\|err^{rel}_{std(e)}\|_2$	$\|err^{rel}_{std(e)}\|_\infty$	$err^{rel}_{\mathbb{E}(y)}$	$err^{rel}_{std(y)}$
Stroud	$1.13 \cdot 10^{-3}$	$6.69 \cdot 10^{-5}$	$7.12 \cdot 10^{-2}$	$1.06 \cdot 10^{-3}$	$8.76 \cdot 10^{-6}$	$4.03 \cdot 10^{-4}$
HGK 0	$6.43 \cdot 10^{-3}$	$7.43 \cdot 10^{-4}$	-	-	$4.58 \cdot 10^{-5}$	-
HGK 1	$1.13 \cdot 10^{-3}$	$6.69 \cdot 10^{-5}$	$7.64 \cdot 10^{-2}$	$1.11 \cdot 10^{-3}$	$8.76 \cdot 10^{-6}$	$4.51 \cdot 10^{-4}$
HGK 2	$1.13 \cdot 10^{-3}$	$6.69 \cdot 10^{-5}$	$7.55 \cdot 10^{-2}$	$1.10 \cdot 10^{-3}$	$8.76 \cdot 10^{-6}$	$4.52 \cdot 10^{-4}$
MC (POD)	$8.79 \cdot 10^{-8}$	$7.35 \cdot 10^{-8}$	$1.83 \cdot 10^{-7}$	$3.04 \cdot 10^{-8}$	$6.96 \cdot 10^{-12}$	$4.10 \cdot 10^{-11}$
Stroud (POD)	$1.13 \cdot 10^{-3}$	$6.69 \cdot 10^{-5}$	$7.12 \cdot 10^{-2}$	$1.06 \cdot 10^{-3}$	$8.76 \cdot 10^{-6}$	$4.03 \cdot 10^{-4}$
HGK 0 (POD)	$6.43 \cdot 10^{-3}$	$7.43 \cdot 10^{-4}$	-	-	$4.58 \cdot 10^{-5}$	-
HGK 1 (POD)	$1.13 \cdot 10^{-3}$	$6.69 \cdot 10^{-5}$	$7.64 \cdot 10^{-2}$	$1.11 \cdot 10^{-3}$	$8.76 \cdot 10^{-6}$	$4.51 \cdot 10^{-4}$
HGK 2 (POD)	$1.13 \cdot 10^{-3}$	$6.69 \cdot 10^{-5}$	$7.55 \cdot 10^{-2}$	$1.10 \cdot 10^{-3}$	$8.76 \cdot 10^{-6}$	$4.52 \cdot 10^{-4}$

Table 2: Relative errors for the coplanar waveguide.

As the electric field is determined on the whole domain, we need to evaluate it in every dof of the FEM grid and compute the relative error locally. This is expressed by writing $e(x)$.

The MC simulation for the reference solution is implemented in MATLAB® and operates on 1 million sample points. The computation took about 10 days on a 64-bit server with CPU type Intel® Xeon® X5650 @2.67GHz, with 2 CPUs, 12 Cores (6 Cores per CPU) and 48 GB main memory available. The variance of the MC with respect to the number of MC sample points is shown in Figure 4. It can be seen that the variance for the electric field e is much higher than for the output y, but both are converging.

The collocation is also implemented in MATLAB. The HGK sparse grids are computed by means of the MATLAB library SGMGA [6]. Table 2 shows the relative errors for mean and standard deviation of e and y.

HGK 0 is not able to approximate the reference solution for the standard deviations since the single grid point is the mean vector of the parameters and hence the standard deviation is zero.
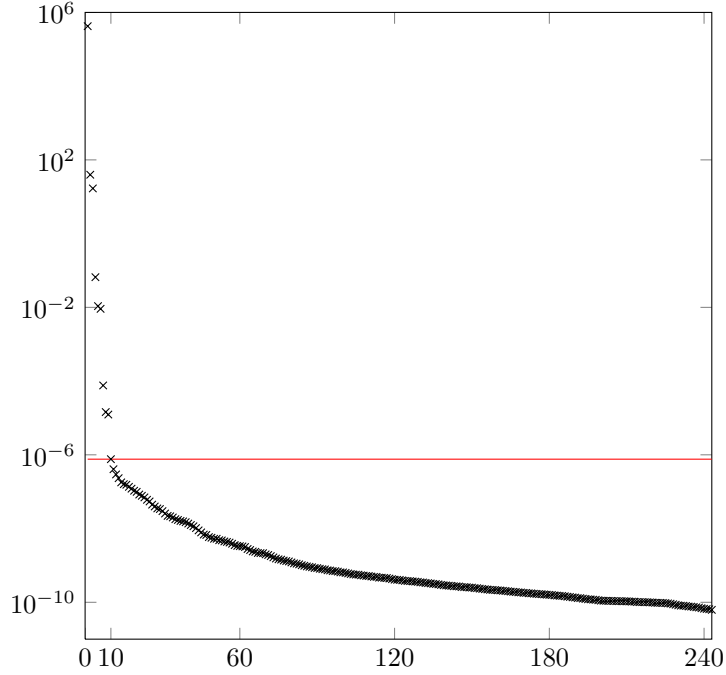
Figure 5: Singular value decay for POD with 3^5 snapshots.

One the other hand, we observe that HGK 1 is already sufficient for this example as there is no considerable improvement when we use HGK 2. Note that HGK 2 consists of 81 grid points. Stroud and HGK 1 are comparable concerning complexity and accuracy.

Using the 3^5 snapshots described in section 4 we achieve the singular value decay shown in Figure 5. We use a POD basis of rank $l = 10$ (see the horizontal line in Figure 5), since the ratio of σ_1 and σ_{10} is already of order 10^{12}. Therefore, the reduced model has dimension 10. The computation of the reduced model could not be done on the same computer as the collocation due to memory requirements. It took about 4 minutes on an Intel®Core2 Duo CPU 3GHz with 4GB RAM available. Considering as deterministic model the system evaluated at the mean of the parameters with solution $\boldsymbol{e}_{full}$ and y_{full}, we can compute the relative errors for the reduced deterministic model with solution $\boldsymbol{e}_{POD}$ and y_{POD}

$$\|err_{\boldsymbol{e}}^{rel}\|_2 := \left\|\frac{\boldsymbol{e}_{full}(\boldsymbol{x}) - \boldsymbol{e}_{POD}(\boldsymbol{x})}{\boldsymbol{e}_{full}(\boldsymbol{x})}\right\|_2 = 9.88 \cdot 10^{-8},$$

$$\|err_{\boldsymbol{e}}^{rel}\|_\infty := \left\|\frac{\boldsymbol{e}_{full}(\boldsymbol{x}) - \boldsymbol{e}_{POD}(\boldsymbol{x})}{\boldsymbol{e}_{full}(\boldsymbol{x})}\right\|_\infty = 7.36 \cdot 10^{-8},$$

$$err_y^{rel} := \left|\frac{y_{full} - y_{POD}}{y_{full}}\right| = 8.22 \cdot 10^{-12}.$$

12

Model \ Method (n)	Stroud (10)	HGK 0 (1)	HGK 1 (11)	HGK 2 (81)	MC (10^6)
FOM (18755 dofs)	23.0	2.3	25.3	186.2	$2.3 \cdot 10^6$
ROM (10 dofs)	$4.6 \cdot 10^{-2}$	$4.6 \cdot 10^{-3}$	$5.1 \cdot 10^{-2}$	$3.7 \cdot 10^{-1}$	$4.6 \cdot 10^3$

Table 3: Computation time in seconds.

Figure 6: $err_{\mathbb{E}(\boldsymbol{e})}^{rel}$ for Stroud, plotted in logarithmic scale.

The deterministic errors are small, which explains that the results for the MC simulation of the reduced model (see Table 2) are even better than the collocation results for the full model. Besides that, the collocation for the reduced model is as good as the collocation for the full model.

The computation time needed for the system evaluations on an Intel®Core2 Duo CPU 3GHz with 4GB RAM available is shown in Table 3. These times confirm that the combination of Stroud or sparse grid based collocation and MOR is a good time-saving alternative for higher dimensional problems. The fact that the errors for the output y are smaller than the ones for the electrical field $\boldsymbol{e}$ for all methods, can be explained by looking at Figure 6 which shows the relative error for the mean of the electric field $\boldsymbol{e}$ computed via Stroud-based collocation on the whole domain G_h and on the left half of the domain. There it can be seen that the error is small in the region around the discrete port which is relevant for the computation of the output y. For comparison, we plotted $err_{\mathbb{E}(\boldsymbol{e})}^{rel}$ for MC of the reduced model in Figure 7. The regions where a visible error occurs are smaller. Both figures have a logarithmic scale and the legends range from the minimum to the maximum of the relative error.

6 Concluding Remarks

In this paper we described several techniques for UQ of the time-harmonic Maxwell's equations. We showed that stochastic collocation is well-suited for the variational analysis of a coplanar waveguide if the collocation points are chosen carefully. Stroud points as well as HGK sparse grid points lead to an efficient computation of the statistical quantities. We compared the results with a very accurate but computationally very costly MC simulation.

On the other hand, we reduced the computation time of the MC simulation by replacing the FOM in the repetitive runs of the deterministic solver by a ROM. This was motivated by the

13

Figure 7: $err^{rel}_{\mathbb{E}(\boldsymbol{e})}$ for MC of the reduced model, plotted in logarithmic scale.

observation that ROMs computed by POD approximate the FOM very well for time-harmonic Maxwells equations with uncertain parameters with small standard deviations. We achieved a high accuracy for ROMs of very small order. Therefore, the combination of MC and MOR turned out to be a good alternative to stochastic collocation based on the FOM.

We also replaced the FOM by a ROM in the stochastic collocation method. This approach does not gain that much from MOR as POD requires more evaluations of the FOM than the collocation itself. This would be different for systems with a higher number of parameters and, thus, a much larger number of collocation points. The application of collocation combined with MOR to examples with many parameters and more degrees of freedom stays future work.

Acknowledgment

References

[1] I. Babuska, F. Nobile, and R. Tempone. A Stochastic Collocation Method for Elliptic Partial Differential Equations with Random Input Data. *SIAM Review*, 52(2):317–355, 2010.

[2] H. Bagci, A. C. Yücel, J. S. Hesthaven, and E. Michielssen. A Fast Stroud-Based Collocation Method for Statistically Characterizing EMI/EMC Phenomena on Complex Platforms. *IEEE Transactions on Electromagnetic Compatibility*, 51(2):301–311, 2009.

[3] O. Bíró. Numerische Aspekte von Potentialformulierungen in der Elektrodynamik. Habilitationsschrift, TU Graz, 1992.

[4] A. Buffa. Trace Theorems on Non-Smooth Boundaries for Functional Spaces Related to Maxwell Equations: an Overview. In P. Monk, C. Carstensen, S. Funken, W. Hackbusch, and R. H. W. Hoppe, editors, *Computational Electromagnetics*, volume 28, pages 23–34. Springer Berlin Heidelberg, 2003.

[5] H.-J. Bungartz and M. Griebel. Sparse grids. *Acta Numerica*, pages 1–123, 2004.

[6] J. Burkardt. SGMGA - Sparse Grid Mixed Growth Anisotropic Rules. `http://people.sc.fsu.edu/~jburkardt/m_src/sgmga/sgmga.html`.

[7] H. C. Elma and Q. Liao. Reduced basis collocation methods for partial differential equations with random coefficients. *SIAM/ASA J. Uncertainty Quantification*, 1(1):192–217, 2013.

[8] A. Ern and J.-L. Guermond. *Theory and Practice of Finite Elements*, volume 159 of *Applied Mathematical Sciences*. Springer–Verlag, Berlin, 2004.

[9] A. Genz and B. D. Keister. Fully symmetric interpolatory rules for multiple integrals over infinite regions with Gaussian weight. *Journal of Computational and Applied Mathematics*, 71:299–309, 1996.

[10] T. Gerstner and M. Griebel. Numerical Integration using Sparse Grids.

[11] G. H. Golub and C. F. Van Loan. *Matrix Computations*. Johns Hopkins Studies in the Mathematical Sciences, 4 edition, 2012.

[12] J. M. Hammersley and D. C. Handscomb. *Monte Carlo Methods*. Methuen, 1964.

[13] J. Horwood, N. Aragon, and A. Poore. Edgeworth Filters for Space Surveillance Tracking. In S. Ryan, editor, *Advanced Maui Optical and Space Surveillance Technologies Conference*, 2010.

[14] F. W. J.Olver. *NIST Handbook of Mathematical Functions*, chapter Quadrature: Gauss–Hermite Formula. Cambridge University Press, 2010.

[15] M. Kahlbacher and S. Volkwein. Galerkin proper orthogonal decomposition methods for parameter dependent elliptic systems. *Discussiones Mathematicae, Differential Inclusions, Control and Optimization*, 27:95–117, 2007.

[16] M. Liu, Z. Gau, and J. S. Hesthaven. Adaptive sparse grid algorithms with applications to electromagnetic scattering under uncertainty. *Applied Numerical Mathematics*, 61:24–37, 2011.

[17] Y. Liu, L. Pileggi, and A. Strojwas. Model order reduction of RC(L) interconnect including variational analysis. In *Proc. Design Automation Conference*, pages 201–206, 1999.

[18] A. Logg, K.-A. Mardal, G. N. Wells, et al. *Automated Solution of Differential Equations by the Finite Element Method*. Springer, 2012.

[19] J. L. Lumley. *Atmospheric turbulence and radio propagation*, chapter The Structure of Inhomogeneous Turbulent Flows, pages 166–178. Publishing House Nauka, 1967.

[20] H. G. Matthies. *Encyclopedia of Computational Mechanics*, chapter Uncertainty Quantification with Stochastic Finite Elements. John Wiley & Sons, Ltd, 2007.

[21] P. Monk. *Finite Element Methods for Maxwell's Equations*. Numerical Mathematics and Scientific Computation. The Clarendon Press Oxford University Press, New York, 2003.

[22] C. Z. Mooney. *Monte Carlo Simulation*. Quantitative Applications in the Social Siences. SAGE University Paper, 116 edition, 1997.

[23] http://www.modelreduction.org.

[24] J.-C. Nédélec. Mixed Finite Elements in R3. *Numer. Math.*, 35:315–341, 1980.

[25] J.-C. Nédélec. A New Family of Mixed Finite Elements in R3. *Numer. Math.*, 50:57–81, 1986.

[26] T. N. L. Patterson. The Optimum Addition of Points to Quadrature Formulae. *Math. Comp.*, 22(104):847–856+s21–s31, 1968.

[27] K. Petras. Smolyak cubature of given polynomial degree with few nodes for increasing dimension. *Numerische Mathematik*, 93(4):729–753, 2003.

[28] R. Pulch, E. J. W. ter Maten, and F. Augustin. Sensitivity analysis and model order reduction for random linear dynamical systems. Preprint BUW-IMACM 13/07, 2013.

[29] P. D. Spanos R. G. Ghanem. *Stochastic Finite Elements: A Spectral Approach*. Springer New York, 1991.

[30] A. E. Ruehli. Equivalent circuit models for three-dimensional multiconductor systems. *IEEE Transactions on Microwave Theory and Techniques*, 22(3), 1974.

[31] C. Schwab and C. J. Gittelson. Sparse tensor discretizations of high-dimensional parametric and stochastic PDEs. *Acta Numerica*, 20:291–467, 2011.

[32] L. Sirovich. Turbulence and the dynamics of coherent structures. partsI-III. *Quart. Appl. Math.*, 45(3):561–590, 1987.

[33] S. Smolyak. Quadrature and interpolation formulas for tensor products of certain classes of functions. *Soviet Math. Dokl.*, 4:240–243, 1963.

[34] A. H. Stroud. Remarks on the Disposition of Points in Numerical Integration Formulas. *Mathematical Tables and Other Aids to Computation*, 11(60):257–261, 1957.

[35] S. Volkwein. Optimal and Suboptimal Control of Partial Differential Equations: Augmented Lagrange-SQP Methods and Reduced-order Modeling with Proper Orthogonal Decomposition. Technical report, Grazer Mathematische Berichte 343, Fachbibliothek für Mathematik, Karl-Franzens-Universität Graz, 2001.

[36] D. Xiu and J. S. Hesthaven. High-Order Collocation Methods for Differential Equations with Random Inputs. *SIAM J. Sci. Comput.*, 27(3):1118–1139, 2005.

[37] S. Zaglmayr. *High Order Finite Element Methods for Electromagnetic Field Computation*. PhD thesis, Johannes Kepler Universität Linz, 2006.